Vietnam Journal of Science and Technology ***58*** *(2) (2020) 204-211*

doi:10.15625/2525-2518/58/2/14225

NO_2 GAS SENSOR BASED ON QCM COATED WITH IRON OXIDE NANORODS[#]

Nguyen Thanh Vinh[1, 2], Vu Ngoc Phan[3], Man Hoai Nam[4], Le Anh Tuan[5], Nguyen Van Quy[1, *]

[1]*International Training Institute for Materials Science, Hanoi University of Science and Technology, No. 1 Dai Co Viet Road, Hai Ba Trung District, Ha Noi, Viet Nam*

[2]*University of Transport Technology, 54 Trieu Khuc, Thanh Xuan District, Ha Noi, Viet Nam*

[3]*Faculty of Biotechnology, Chemistry and Environmental, Phenikaa University, Ha Noi, Viet Nam*

[4]*Institute of Materials Science, Vietnam Academy of Science and Technology, 18 Hoang Quoc Viet Road, Cau Giay, Ha Noi, Viet Nam*

[5]*Phenikaa University Nano Institute, Phenikaa University, Ha Dong, Ha Noi, Viet Nam*

[*]Email: *quy@itims.edu.vn; quy.nguyenvan@hust.edu.vn*

Received: 16 August 2019; Accepted for publication: 27 October 2019

Abstract. Iron oxide nanorods were synthesized by chemical co-precipitation method. The structural and morphological characteristics of the as-synthesized nanorods were analyzed by X-ray diffraction (XRD) and scanning electron microscopy. The results show that the iron oxide nanorods include the mixture of Fe_3O_4, γ-Fe_2O_3 and FeOOH with the diameter and the length of iron oxide nanorods to be 30 and 100 nm, respectively. The iron oxide nanorods were then dispersed and deposited on the gold electrode of quartz crystal microbalance (QCM) for the gas sensor. The iron oxide nanorods based QCM sensor was tested with various concentrations of numerous toxic gases at room temperature, including nitrogen dioxide (NO_2), sulfur dioxide (SO_2), ammonia (NH_3), and carbon monoxide (CO). The testing results indicate that the fabricated sensor exhibits high sensing performance to NO_2 gas in the concentration range from 5 to 20 ppm.

Keywords: QCM, NO_2, gas sensor, iron oxide, nanorods.

Classification numbers: 2.4.2, 2.5.3, 3.2.3.

1. INTRODUCTION

Nowadays, rapid and continuous development of industries and motor vehicle is the main emission sources of toxic and hazardous gases such as nitrogen dioxide (NO_2), sulfur dioxide (SO_2), ammonia (NH_3) and carbon monoxide (CO). Due to the large emission, these gases cause greenhouse effect, melting glaciers, acid rain, ozone layer depletion, photochemical smog, and

[#] Presented at the 11th National Conference on Solid State Physics & Materials Science, Quy Nhon 11-2019.

corrosion of metal [1]. Among toxic gases, NO_2 is an oxidizing gas which is disposed into the atmosphere from the fossil fuel combustion in vehicle's engines and industrial activities. They are the main cause of respiratory diseases or death when exposure of creature to several ppm of nitrogen dioxide. Moreover, nitrogen dioxide is recognized as a typical air pollutant [2]. Therefore, the development of gas sensors with high sensitivity at low concentration of NO_2 gas is very essential [1-4].

The problem of environmental pollution's detection and treatment has attracted much concern from many scientists all over the world, and one of the current solutions is to use nanomaterials in the physical, chemical and environmental fields [5-7]. Nowadays, several types of gas sensor are investigated for detection, analysis and measurement of the toxic gas, including the sensors based on resistance change, optics, electrochemistry, MEMS, and mass. The gas sensors based on the resistance change using semiconductor metal oxide materials are one of the most popular types [8-11]. However, these gas sensors have a few drawbacks, for example only working effectively at high temperature. The sensors based on optical principle usually use expensive equipment and complex optical systems [12], The MEMS type based sensors require complex fabrication system with high cost [13]. Among the plurality of gas sensor systems used for toxic gas monitoring, a quartz crystal microbalance (QCM) is not the only mass sensor but also the system attracting more special attentions. The gas sensor based on QCM is an important and promising sensing system for the real-time detection of toxic gases, in which the sensor can change of resonance frequency when a small mass is adsorbed on the piezoelectric quartz crystal, and the QCM has a special advantage of high sensitivity for working at room temperature. Besides, the QCM can be combined with many various sensing materials such as polymers [14], carbon nanotubes (CNTs) [15], graphene [16] for sensing application. Moreover, the QCM has been applied in many fields as humidity sensor [17], sensor of volatile organic compounds (VOCs) [18], sensor of toxic gases SO_2 [19-21], NO_2 [1-4], and CO [22]. These published results indicated that sensing material layer on the gold electrode is the important key of the QCM sensors.

In our study, we focused on the synthesis of iron oxide by the chemical co-precipitation method. The properties of the iron oxide nanorods were characterized by field-emission scanning microscopy (FE-SEM) and X-ray diffractometer (XRD). The iron oxide nanorods were used as a sensing material layer for QCM gas sensor due to their special characteristics, including low-cost and excellent catalytic activity [23], high density of active groups (OH) [24], which promise excellent gas sensitivity properties of the QCM sensor. Moreover, the iron oxide is a popular semiconducting metal oxide material with easy fabrication. Hence, the NO_2 gas sensor based on QCM coated with the iron oxide nanorods was developed.

2. MATERIALS AND METHODS

Chemical reagents of $FeCl_3.6H_2O$, $FeCl_2.4H_2O$, and NaOH were purchased from Xilong Scientific Co., Ltd (Guangdong, China). Iron oxide nanomaterials were fabricated by the procedure of the experiment described in Fig. 1. The chemical reaction performed according to the equation [25]:

$$Fe^{2+} + Fe^{3+} + OH^- \rightarrow Fe_3O_4 + H_2O \quad (1)$$

at first, 3.175 g of $FeCl_2.4H_2O$ and 8.125 g of $FeCl_3.6H_2O$ were dispersed in 100 ml deionized water by the aid of a magnetic stirrer. After that, the temperature of the solution was raised to

0 °C. The NaOH solution of 2 M was then slowly added to the prepared solution at the rate of 1 ml/min. The mixture solution was continued stirring in N_2 ambient environment until the solution changed from orange to black. Iron oxide nanorods were collected by using a magnet and washed with deionized water until to get pH of 7. The iron oxide nanorods were dried in an oven at 80 °C for 20 h. The morphology and crystallinity of the nanorods were characterized by field-emission scanning microscopy (FE-SEM) and X-ray diffractometer (XRD).

In order to fabricate the sensor, a 0.2 g of the iron oxide nanorods was dispersed in 20 ml deionized water by the aid of ultrasonic vibrating device at 120 W for 30 min. The QCM was coated with 3 ml dispersion solution of iron oxide nanomaterials by spray-coating method at the rate of 0.2 ml min^{-1}. The gas sensing properties of the fabricated sensor were tested with the various concentrations of toxic gases by using a home-made measurement system. The detail of the gas sensing measurement was presented in our previous work [15]. In brief, all the measurements were carried out at room temperature. Dry air and testing gas flows were kept at a constant flowrate of 200 sccm. The change in frequency of the sensor was monitored by a QCM200 system linked to PC via the SRSQCM200 software program.

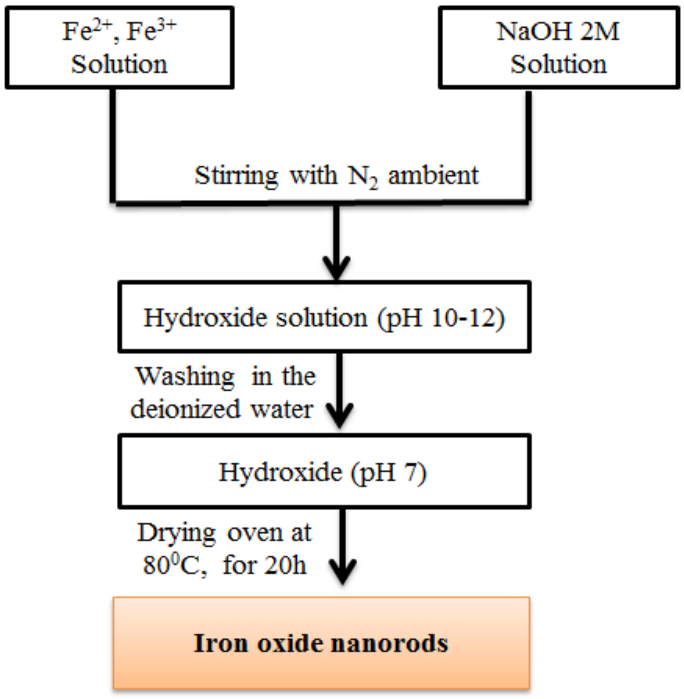

Figure 1. Diagram of experimental steps.

3. RESULTS AND DISCUSSION

Figure 2 shows SEM images of the as-grown (Fig. 2a) and dispersed films (Fig. 2b) of the iron oxide nanorods. The result shows that the morphology of the iron oxide nanorods has no change after dispersing in the deionized water and depositing on the gold electrode of QCM. The average length of iron oxide nanorods is 100 nm and the diameter is from 30 to 50 nm. Fig. 2 also indicates that the layer of the iron oxide nanorods is disorder with many holes, which may increase the adsorption capacity of the gas molecules on its surface. Thus, the rods occupy a

small area on the active electrode of the sensor but they still have a large surface area. Hence, the sensing layer exposes high porosity and large effective area. The SEM results exhibited that the gas sensor based on the iron oxide nanorods can achieve a high gas sensing performance.

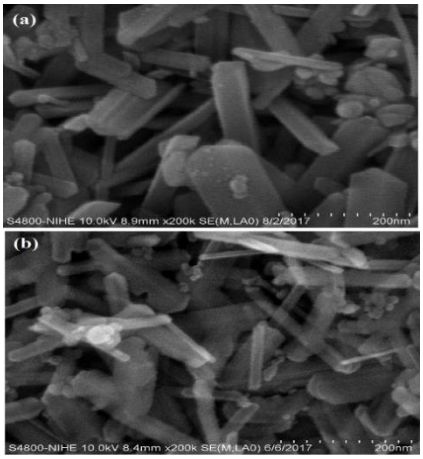

Figure 2. SEM images of the iron oxide nanorods before (a) and after (b) deposited on the QCM.

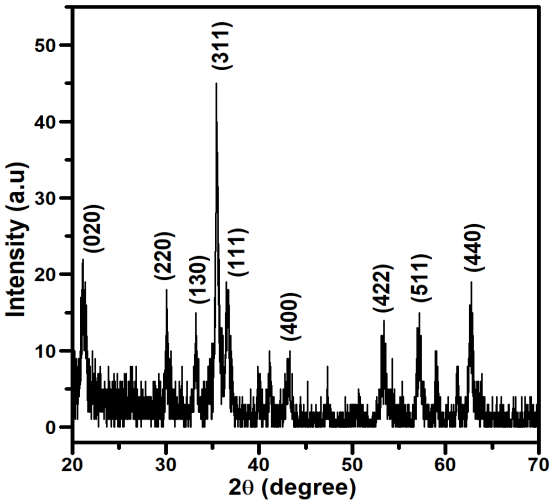

Figure 3. XRD pattern of the iron oxide nanorods.

Figure 3 shows XRD pattern of the iron oxide nanorods recorded in the 2θ from 20 to 70°. All the strongest diffraction peaks were assigned to the standard cards of Fe_3O_4 [JCPDS card No.19-0629], γ-Fe_2O_3 [JCPDS card No. 39.1346]. The diffraction peaks of (220), (311), (400), (422), (511), and (440) planes match well the crystals of Fe_3O_4 and γ-Fe_2O_3. However, it is difficult to identify unambiguously the phase composition of the samples by X-ray diffraction [26] because these planes are the same for Fe_3O_4 and γ-Fe_2O_3 [25]. In our work, the iron oxide nanorods were dried in ambient air at 80 °C in the last step of experimental process. Hence, a part of Fe_3O_4 could transferred to γ-Fe_2O_3. Moreover, the diffraction peaks of (020), (130), and (111) planes are the characteristic peaks to identify α-FeOOH [11,27]. Therefore, the XRD result illustrated that the synthesized iron oxide nanorods were a mixture of Fe_3O_4, γ-Fe_2O_3, and α-FeOOH.

In order to study the gas sensing properties, the sensor was tested with the various toxic gases. The results expose that the fabricated sensor has good sensitivity with NO_2 gas. Fig. 4 shows the comparison of the frequency shift of QCM sensor when exposed to several gases, including NH_3, CO, SO_2 and NO_2. Namely, the frequency shift of the sensor is 1.2, 2.0, 2.5, and 3.7 Hz when exposed to the 250 ppm of NH_3, 100 ppm of CO, and 15 ppm of SO_2 and NO_2, respectively. The relation between the change in the resonant frequency of a QCM and the mass of gases adsorbed on the iron oxide nanorods can be calculated according to the Sauerbrey equation as follows [28].

$$\Delta f = \frac{-2f_0^2}{A\rho_q}\Delta m, \quad (1)$$

where A is the active area of the QCM electrode in cm^2, f_0 is the resonant frequency of the QCM in Hertz (Hz), Δm is the change in the oscillating mass in grams (g), ρ_q is the density of quartz, and v_q is the shear wave velocity in the quartz.

The gas sensing properties of the QCM based sensor are summarized in Table. 1. It can be seen that the frequency shift of the sensor with NO_2 is the highest with value of 0.247 Hz/ppm. The results demonstrate that the mass of NO_2 adsorbed on the sensor surface is the largest in comparison with the four gases. Therefore, the QCM sensor coated with a thin layer of iron oxide nanorods on the gold electrode shows high selectivity for nitrogen dioxide. Although the molecular weight of NO_2 is smaller than that of SO_2 ($m_{NO_2} = 46$ and $m_{SO_2} = 64$), the frequency shift of the sensor with NO_2 gas is higher than that of SO_2 at the same concentration. This phenomenon could be explained by the natural properties of nitrogen dioxide: at high density, the NO_2 molecules can exist as dimers ($NO_2 + NO_2 \rightleftarrows N_2O_4$, $m_{N_2O_4} = 92$) [1] that causes NO_2 gas to be the highest sensitivity.

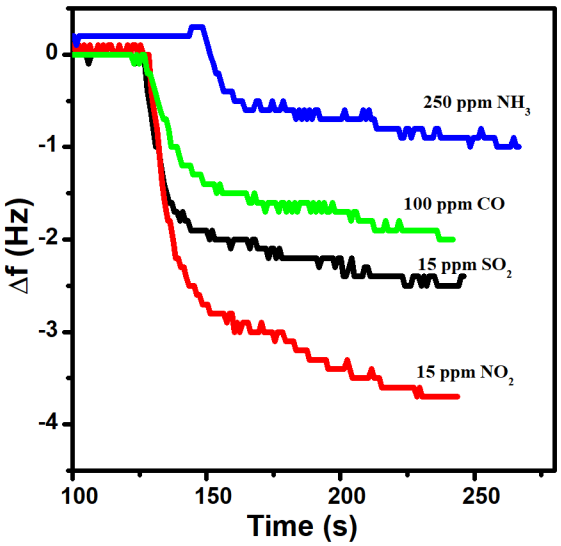

Figure 4. Frequency shift of the QCM sensor when exposed to NH_3, CO, SO_2, and NO_2 gases.

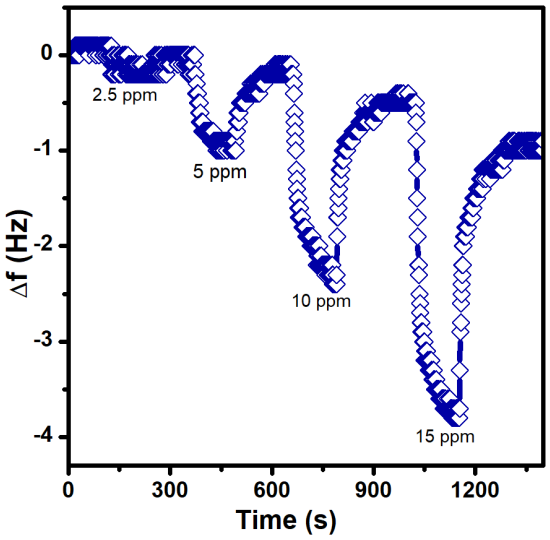

Figure 5. Frequency shift of the QCM sensor with different NO_2 concentrations.

Table 1. The comparison of gas sensitivity factor of the QCM sensor.

Gas	Sensitivity factor (Hz/ppm)
NH_3	0.005
CO	0.020
SO_2	0.167
NO_2	0.247

Figure 5 illustrates the response and recovery curve of the QCM sensor at various concentrations of NO_2 gas with the range from 2.5 ppm to 15 ppm at room temperature. In the first stage, the sensor was flushed with a reference N_2 gas flow of 200 sccm to obtain a baseline. Next, the QCM sensor was exposed to 2.5 ppm of NO_2, the flow rate of the mixture gas of NO_2\$N_2$ was also kept constant at 200 sccm. After the response-recovery curves reached saturation state, the mixture gas of NO_2\$N_2$ was replaced by 200 sccm of N_2 gas and the resonant frequency of the QCM sensor increased and returned to its baseline. Similarly, testing gas process continues to be repeated at other concentrations of 5, 10, and 15 ppm. It can be clearly seen that, the frequency shift of the QCM sensor increases linearly with an increasing

concentrations of NO_2 gas. Namely, the frequency shift of the sensor is 0.2, 1, 2.42 and 3.45 Hz at NO_2 gas concentrations of 2.5, 5, 10, and 15 ppm, respectively.

To study the repeatability of the sensor, the response curves of the fabricated QCM sensor were tested at 10 ppm and 15 ppm NO_2 gas at room temperature for four cycles, as shown in Fig. 6. Fig. 6 shows that the sensor exposes a good repeatability and reversibility for four times. The frequency shift of the sensor exhibits to be similar behavior to the results described in Fig. 5.

In order to investigate the response and recovery times of the sensor, the frequency shift versus time at different concentrations of NO_2 is described in Fig 7. In this case, the response time is defined by time to reach 90% variation in the frequency shift maximum upon exposed to the gas ($\tau_{N_2-NO_2}$), and recovery time is time reverted to 90% resonance frequency of the sensor at the baseline value ($\tau_{NO_2-N_2}$). The result from Fig. 7 shows that the response time of the iron oxide nanorods coated QCM sensor is 46, 61 and 73 s when the sensor exposed to 5, 10 and 15 ppm, respectively. Additionally, the average recovery time in all testing gases increased from 35 to 86 s. The speed of response time and the speed of the recovery time rose with an increasing concentration of NO_2 gas, as shown in Table. 2. Hence, NO_2 molecules easily adsorb on surface of the iron oxide nanorods and fast desorption at high concentration of NO_2. The testing results exhibited that the iron oxide nanorods-coated on gold electrode of QCM had a good reproducibility reversibility as well as fast response-recovery behavior for NO_2-sensing.

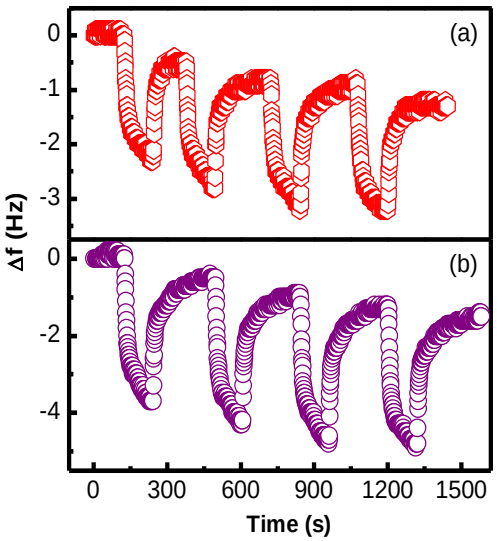

Figure 6. Repeatability response curves of the QCM sensor (a) at 10 ppm and (b) at 15 ppm of NO_2 for four cycles.

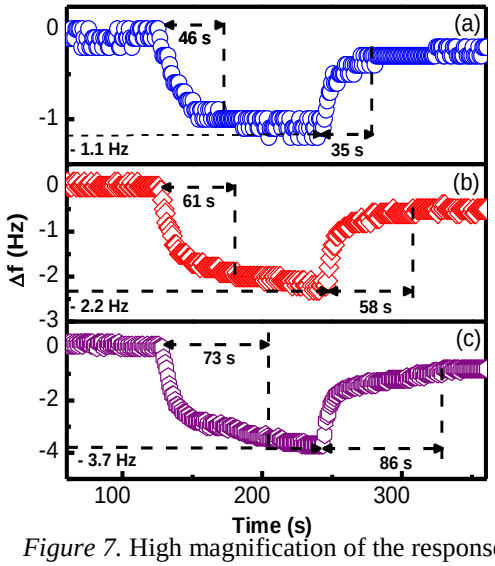

Figure 7. High magnification of the response and recovery times of the QCM sensor to (a) 5 ppm, (b) 10 ppm, (c) 15 ppm. of NO_2.

Table 2. The response and recovery times of the QCM sensor.

Con. (ppm)	Response time		Recovery time	
	$\tau_{N_2-NO_2}$ (Hz)	Speed (Hz/s)	$\tau_{NO_2-N_2}$ (Hz)	Speed (Hz/s)
5	46	0.021	35	0.023
10	61	0.032	58	0.028
15	73	0.046	86	0.034

4. CONCLUSIONS

In summary, the iron oxide-hydroxide nanorods were successfully synthesized by co-precipitation method. A porous layer of the iron oxide nanorods was sprayed on the QCM as a room temperature gas sensor for detection of NO_2 gas. The fabricated sensor indicated good response at the lowest NO_2 gas concentration of 2.5 ppm. The frequency shift of the sensor linearly increases with an increase in NO_2 gas concentration in the range of 2.5 - 15 ppm. The gas sensing results suggested that the QCM sensor with the thin layer of the iron oxide nanorods exhibited good repeatability, reversibility and stability. Moreover, the sensor exposes high sensitivity and selectivity to NO_2 gas. Hence, the QCM sensor coated with the iron oxide-hydroxide showed an ability of high NO_2 gas sensing performance in the future.

Acknowledgements. This research was supported by grant No. 103.02-2015.08 from the research program of Vietnam National Foundation for Science and Technology (NAFOSTED).

REFERENCES

1. Matsuguchi M., Kadowaki Y., Tanaka M. - A QCM-based NO_2 gas detector using morpholine-functional cross-linked copolymer coatings, Sensors and Actuators B: Chemical **108** (2005) 572-572.
2. Jung W., Sahner K., Leung A., Tuller H. L. - Acoustic wave-based NO_2 sensor: Ink-jet printed active layer, Sensors and Actuators B: Chemical **141** (2009) 485-490.
3. Gu D., Li X., Zhao Y., Wang J. - Enhanced NO_2 sensing of SnO_2/SnS_2 heterojunction based on sensor, Sensors and Actuators B: Chemical **244** (2017) 67-76.
4. Georgieva V., Mitkova M., Chen P., Tenne D., Wolf K., Gadjanova Victoria - NO_2 gas sorption studies of $Ge_{33}Se_{67}$ films using quartz crystal microbalance, Materials Chemistry and Physics **137** (2012) 552-557.
5. Dulian P., Nachit W., Jaglarz J., Zieba P., Kanak J., Zukowski W. - Photocatalytic mythylene blue degradation on multilayer transparent TiO_2, Optical Materials **90** (2019) 264-272.
6. Cao Z., Guo J., Fan X., Xu J., Fan Z., Du B. - Detection of heavy metal ions in aqueous solution by P(MBTVBC-co-VIM)-coated QCM sensor, Sensors and Actuators B: Chemical **157** (2011) 34-41.
7. Lee S. J., Eom A. H., Ryu S., Won J. P. - Resistance of an eco-friendly nano-polymer fireproof cementitious composite to physical and chemical environment, Composite Structures **22** (2019) 110901.
8. Zhang H. J., Meng F. N., Liu L. Z., Chen Y. J. - Convenient route for synthesis of alpha-Fe_2O_3 and sensors for H_2S gas, Journal of Alloys and Compounds **774** (2018) 1181-1188.
9. Zhang C., Luo Y., Xu J., Debliquy M. - Room temperature conductive type metal oxide semiconductor gas sensors for NO_2 detection, Sensors and Actuators A: Physical **289** (2019) 118-133.
10. Kamble C., Panse M. - IDE Embedded Tungsten Trioxide Gas sensor for sensitive NO_2 detection, Materials Chemistry and Physics **224** (2018) 257-263.
11. Patil D., Patil V., Patil P. - Highly sensitive and selective LPG sensor based on α-Fe_2O_3 nanorods, Sensors and Actuators B: Chemical **152** (2011) 299-302.
12. Zhang M., Li J. - Synthesis and Characterization of a Novel Porphyrin Derivative for Optical Sensor, Materials Letters **247** (2019) 119-121.

13. Gerdroodbary M. B., Ganji D. D., Shiryanpour I., Moradi R. - Mass analysis of CH_4/SO_2 gas mixture by low-pressure MEMS gas sensor, Journal of Natural Gas Science and Engineering **53** (2018) 317-328.
14. Sroysee W., Chunta S., Amatatongchai M., Lieberzeit P. A. - Molecularly imprinted polymers to detect profenofos carbonfuran selectively with QCM sensors, Physics in Medicine **7** (2019) 100016.
15. Hoang N. D., Cat V. V., Nam M. H., Phan V. N., Le A. T., Quy N. V. - Enhanced SO_2 sensing characteristics of Multi-wall carbon nanotubes based mass-type sensor using two-step purification process, Sensors and Actuators A: Physical **295** (2019) 696-702.
16. Lee S. W., Choi B. I., Kim J. C., Woo S. B., Kim Y. G. - Reduction and compensation of humidity measurement errors at cold temperatures using dual QCM humidity sensors based on Graphene oxide, Sensors and Actuators B: Chemical **284** (2019) 386-394.
17. Qi P., Zhang T., Shao J., Yang B., Fei T., Wang R. - A QCM humidity sensor constructed by graphene quantum dots and chitosan composites, Sensors and Actuators A: Physical **297** (2019) 93 – 101.
18. Dinh N. X., Le A. T., Quy N. V. - Room Temperature Violate Organic Compound Sensor Based on Functional Multi-Wall Carbon Nanotubes Coated Quartz Crystal Microbalance, Sensors Letters **13** (2015) 499-455.
19. Tian Y., Qu K., Zeng X. - Investigation into the Ring-Substituted Polyanilines and Their Application for the Detection and Adsorption of Sulfur Dioxide, Sensors and Actuators B: Chemical **249** (2019) 423-430.
20. Syritski V., Reut J., Opik A., Idla K. - Environmental QCM sensors coated with polypyrrole, Synthetic Metals **102** (1999) 1326 – 1327.
21. Matsuguchi M., Tamai K., Sakai Y. - SO_2 gas sensors using polymers with different amino groups, Sensors and Actuator B: Chemical **77** (2001) 363 - 367.
22. Ozbek C., Okur S., Mermer O., Kurt M., Sayin S., Yilmaz M. - Effect of Fe doping on the CO gas sensing of functional calixarene molecules measured with quartz crystal microbalance technique, Sensors and Actuators B: Chemical **215** (2015) 464-470.
23. Li C., Wu J., Peng W., Fang Z., Liu J. - Peroxy monosulfate activation for efficient sulfamethoxazole degradation by Fe_3O_4/β-FeOOH nanocomposites: coexistence of radical and non-radical reactions, Chemical Engineering Journal **306** (2018) 904-914.
24. Wang C., Li A., Shuang C. - The effect on ozone catalytic performance of prepared-FeOOH by different precursors, Journal of Environmental Management **228** (2018) 158-164.
25. Zhang L., Huang Z., Shao H., Li Y., Zheng H. - Effects of γ-Fe_2O_3 on γ-Fe_2O_3/Fe_3O_4 composite magnetic fluid by low-temperature low-vacuum oxidation method, Materials and Design **105** (2016) 234-239.
26. Lukashova N., Savchenko A., Yagodkin Y., Muradova A.G., Yurtov E.V. - Investigation of structure and magnetic properties of nanocrystalline iron oxide for use in magnetic fluids, Journal of Alloys and Compounds **586** (2014) S298 – S300.
27. Khder A., Ashour S., Altass H., Khairou K. - Pd nanoparticles supported on iron oxide nanorods for CO oxidation: Effect of preparation method, Journal of Environmental Chemical Engineering **4** (2016) 4794 – 4800.
28. Sauerbrey G. - The use of quartz crystal oscillators for microweighing, Z. Phys **155** (1959) 206.